

Cite this: *Chem. Sci.*, 2020, **11**, 551

All publication charges for this article have been paid for by the Royal Society of Chemistry

Received 7th October 2019
Accepted 23rd November 2019

DOI: 10.1039/c9sc05026d
rsc.li/chemical-science

Introduction

Cyclic (alkyl)(amino)carbenes (CAACs) have become the ligands of choice for the stabilisation of many main group compounds in low oxidation states owing to their excellent σ -donor and π -acceptor properties derived from a relatively high-lying HOMO and low-lying LUMO.^{1–4} In the field of low-valent mononuclear boron chemistry, they have been successfully employed to synthesise unusual boron(II) species such as boryl radicals $[(\text{CAAC})\text{BX}_Y]^{\bullet}$; X, Y = anionic ligands, *e.g.* **I**, Fig. 1a),^{5–10} boryl radical cations $[(\text{CAAC})\text{LBY}]^{\bullet+}$, L = Lewis donor^{10–13} and boryl anions $[(\text{CAAC})\text{BX}_Y]^-$, *e.g.* **II**,^{14–17} as well as boron(I) species such as borylenes $[(\text{CAAC})\text{LBX}]$, *e.g.* **III**, and $(\text{CAAC})\text{BNR}_2$.^{6–8,11–13,16,18–20} In all these compounds, the accumulation of negative charge on the low-valent boron centre is stabilised through π back-bonding to the CAAC ligand(s) (Fig. 1a), making many of them surprisingly stable under inert conditions.^{1–4} Recently, transient dicoordinate (CAAC)-stabilised borylenes have drawn particular attention as compounds capable of activating and catenating N_2 ,^{21–25} the latter reaction being unprecedented even in transition metal chemistry.

Furthermore, CAACs have been shown to activate element–hydrogen σ bonds, including H–H, N–H, P–H, Si–H and B–H by addition to their nucleophilic carbene carbon.^{3,4} In CAAC-

supported hydroboron compounds, the B–H bond activation process can be reversible (Fig. 1b)^{14,26,27} and is favoured by electron-donating ligands at boron,^{8,26–30} thereby affording additional stabilisation for electron-rich lower oxidation state species through facile hydrogen shuttling. In this contribution we combine the excellent σ -donating/ π -accepting and B–H bond activating properties of CAACs to synthesise and isolate a solvent-free alkyl(hydro)boryl anion, and selectively oxidise it to the corresponding radical, which is surprisingly air-stable in the solid state.

Results and discussion

Following a procedure by Bertrand and co-workers,¹² methyl trifluoromethanesulfonate (MeOTf) was employed to abstract a hydride from $(\text{CAAC}^{\text{Me}})\text{BH}_3$ ($\text{CAAC}^{\text{Me}} = 1\text{-(2,6-diisopropylphenyl)-3,3,5,5-tetramethylpyrrolidin-2-ylidene}$). The resulting triflate derivative **1** was treated in a 1 : 1 ratio with a series of Lewis bases in benzene to generate the bis(base)-stabilised boronium cations $[(\text{CAAC}^{\text{Me}})\text{BH}_2\text{L}]^{\bullet+}$ (2–L, L = CAAC^{Me} , $\text{IMe}^{\text{Me}} = 1,3\text{-dimethylimidazol-2-ylidene}$, PMe_3 , Scheme 1a), all presenting a characteristic upfield ^{11}B NMR BH_2 triplet in the –22 to –30 ppm region.⁸ In the case of the 4-dimethylaminopyridine (DMAP) derivative, **2-DMAP** ($\delta^{11}\text{B} = -10.6$ ppm, broad), the synthesis had to be carried out in THF as treatment of **1** with one equivalent of DMAP in benzene resulted in the formation of the bis(DMAP) adduct **3-DMAP** ($\delta^{11}\text{B} = 4.2$ ppm, Scheme 1b), in which the second DMAP equivalent has promoted a typical 1,2-migration of one hydrogen atom from boron to the CAAC^{Me} ligand.²⁶ The solid-state structure of **3-DMAP** (Fig. 2) evidences the binding of the DMAP residues and the migration of H1 to C1, which is now sp^3 -hybridised (B1–C1 1.619(4), C1–N1 1.490(3) Å). In contrast, the binding of a second equivalent of pyridine to **2-Pyr** ($\delta^{11}\text{B} = -9.3$ ppm,

^aInstitut für Anorganische Chemie, Julius-Maximilians-Universität Würzburg, Am Hubland, 97074 Würzburg, Germany. E-mail: h.braunschweig@uni-wuerzburg.de

^bInstitute for Sustainable Chemistry & Catalysis with Boron, Julius-Maximilians-Universität Würzburg, Am Hubland, 97074 Würzburg, Germany

^cInstitut für Physikalische und Theoretische Chemie, Julius-Maximilians-Universität Würzburg, Emil-Fischer-Straße 42, 97074 Würzburg, Germany

† Electronic supplementary information (ESI) available: Synthetic procedures, NMR, EPR, UV-vis, IR, CV, X-ray crystallographic data and details of the computational analyses. CCDC 1956847–1956854. For ESI and crystallographic data in CIF or other electronic format see DOI: 10.1039/c9sc05026d



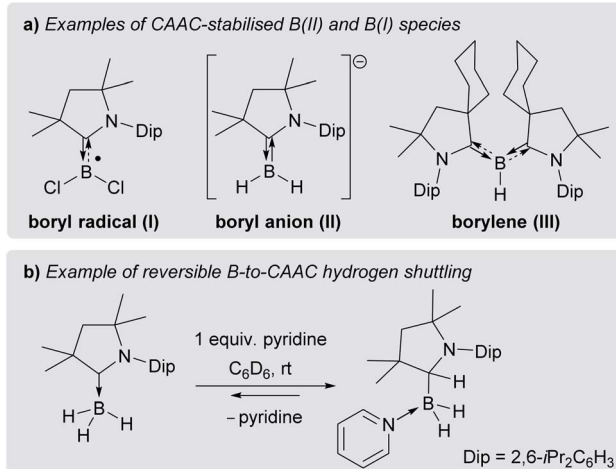
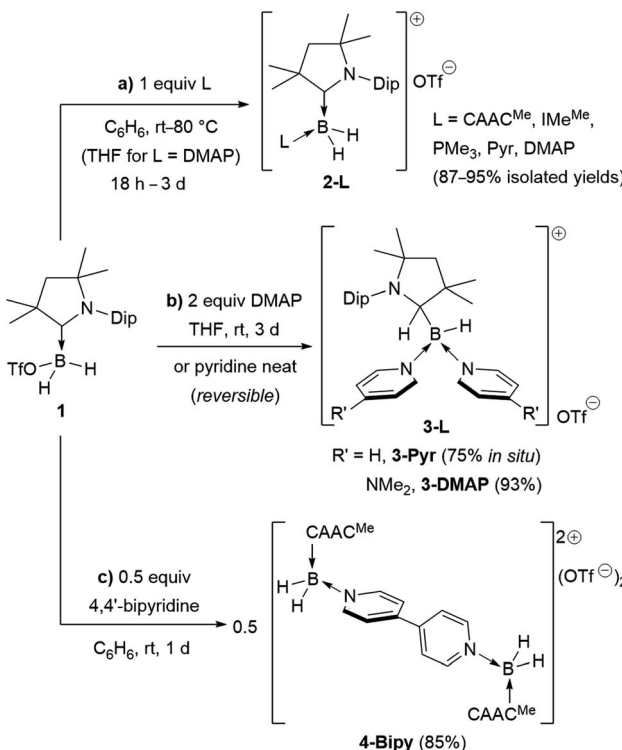


Fig. 1 (a) Selected examples of CAAC-stabilised B(II) and B(I) species; (b) example of reversible Lewis-base-induced B-to-CAAC hydrogen shuttling.

broad) was found to be reversible: even in neat pyridine only *ca.* 75% conversion to **3-Pyr** ($\delta_{11\text{B}} = 6.9$ ppm) was observed. The use of 4,4'-bipyridine as a base led to the formation of the 4,4'-bipyridine-bridged bis(boronium) species **4-Bipy** ($\delta_{11\text{B}} = -8.6$ ppm, broad, Scheme 1c). Attempts to synthesise the derivative **2-thf** in THF resulted in ring-opening polymerisation of the solvent within two days at room temperature.



Scheme 1 Syntheses of bis- and tris(base)-stabilised boronium cations (a) **2-L**, (b) **3-L** and (c) **4-L**. Isolated yields in brackets. IMe^{Me} = 1,3,4,5-tetramethylimidazol-2-ylidene, Pyr = pyridine, DMAP = 4-dimethylaminopyridine.

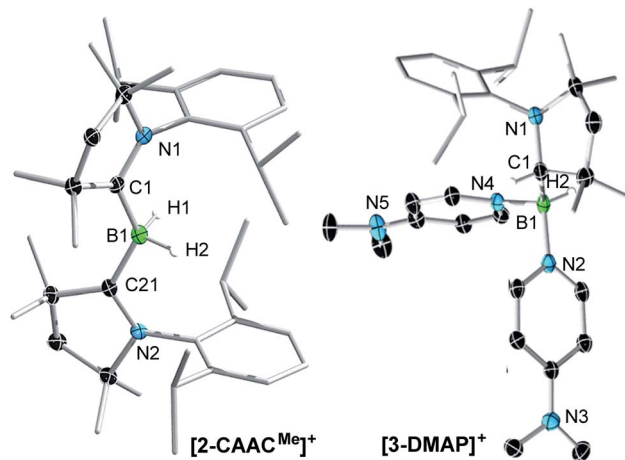
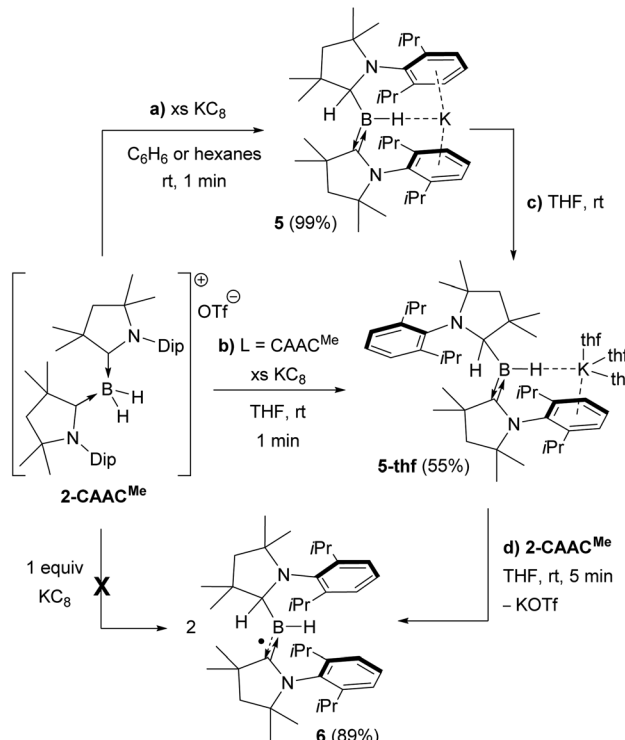


Fig. 2 Crystallographically derived molecular structures of the **2-CAAC^{Me}** (one of the two crystallographically distinct cations present in the asymmetric unit) and **3-DMAP** cations. Atomic displacement ellipsoids are set at 50% probability. Ellipsoids of CH₃ and iPr groups, triflate counteranion and hydrogen atoms omitted for clarity except for boron-bound hydrides.‡ Selected bond lengths (Å) for **2-CAAC^{Me}**: B1-C1 1.597(7), B1-C21 1.607(7), B1-H1 1.11(6), B1-H2 1.16(6), C1-N1 1.316(6), C21-N2 1.310(6); for **3-DMAP** B1-C1 1.619(4), B1-N2 1.585(3), B1-N4 1.597(3), B1-H2 1.10(2), C1-N1 1.490(3).

Attempts to reduce **2-L**, **3-L** and **4-L** under various conditions all resulted in unselective reactions, except for **2-CAAC^{Me}**, which was readily reduced with excess KC₈ to the red-coloured (alkyl) hydroboryl anion **5** by 1,2-migration of one hydrogen atom from boron to CAAC^{Me} (Scheme 2a). The ¹¹B NMR spectrum of 5



Scheme 2 Reduction of **2-CAAC^{Me}** to boryl anions (a) **5** and (b)-(c) **5-thf**, and subsequent comproportionation to (d) boryl radical **6**.



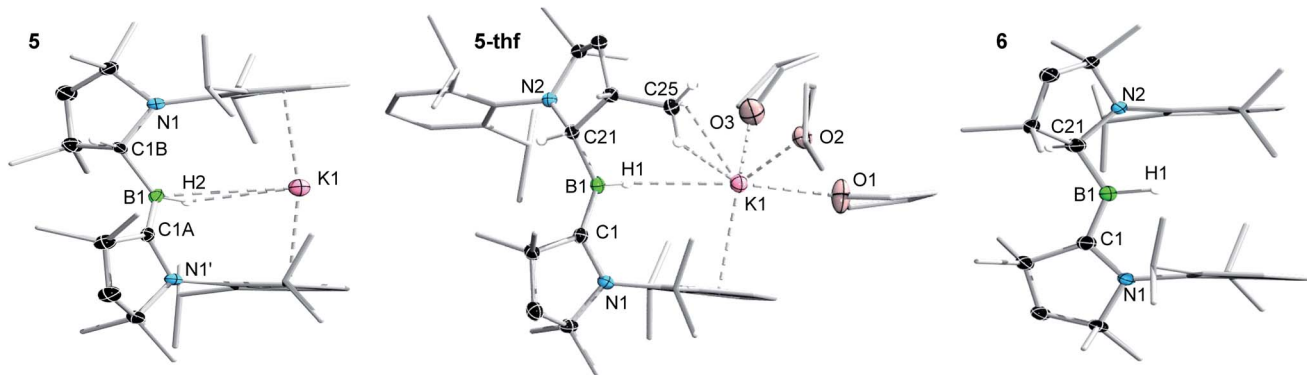


Fig. 3 Crystallographically derived molecular structures of **5**, **5-thf** and **6**. Atomic displacement ellipsoids are set at 50% probability. Ellipsoids of CH_2 , CH_3 and iPr groups and hydrogen atoms omitted for clarity except for boron-bound hydrides.[‡] Selected bond lengths (Å) and angles ($^\circ$) for **5**: $\text{B1}-\text{C1A}$ 1.439(11), $\text{B1}-\text{C1B}$ 1.633(9), $\text{B1}-\text{H2}$ 1.14(3), $\text{C1A}-\text{N1}'$ 1.450(7), $\text{C1B}-\text{N1}$ 1.520(8), $\text{K1}\cdots\text{H1}$ 2.53(3), $\text{K1}\cdots\text{B1}$ 3.141(4), $\text{K1}\cdots\text{centroid}$ 2.91, $\Sigma\angle\text{B1}$ 359.4(12), $\Sigma\angle\text{C1A}$ 359.7(5), $\text{B1}-\text{H2}-\text{K1}$ 111.8(12); for **5-thf**: $\text{B1}-\text{C1}$ 1.452(2), $\text{B1}-\text{C21}$ 1.620(2), $\text{B1}-\text{H1}$ 1.159(17), $\text{C1}-\text{N1}$ 1.4601(18), $\text{C21}-\text{N2}$ 1.5076(19), $\text{K1}\cdots\text{H1}$ 2.653(16), $\text{K1}\cdots\text{B1}$ 3.599(2), $\text{K1}\cdots\text{centroid}$ 2.95, $\text{K1}\cdots\text{C25}$ 3.2933(17), $\Sigma\angle\text{B1}$ 359.9(1), $\Sigma\angle\text{C1}$ 359.9(1), $\text{B1}-\text{H1}-\text{K1}$ 138(1); for **6**: $\text{B1}-\text{C1}$ 1.5174(18), $\text{B1}-\text{C21}$ 1.5817(18), $\text{B1}-\text{H1}$ 1.142(18), $\text{C1}-\text{N1}$ 1.3777(15), $\text{C21}-\text{N2}$ 1.4616(15), $\Sigma\angle\text{B1}$ 359.5(6), $\Sigma\angle\text{C1}$ 359.6(1).

shows a single broad resonance at 16.7 ppm, significantly downfield-shifted from that of other CAAC-stabilised boryl anions, which range from $\delta^{11}\text{B} = -4.7$ ppm for $[(\text{CAAC}^{\text{Me}})\text{BH}_2]^-$ to $\delta^{11}\text{B} = -17.9$ ppm for $[(\text{CAAC}^{\text{Cy}})\text{B}(\text{CN})_2]^-$,¹⁴⁻¹⁷ likely because of the electron-withdrawing nature of the aminoalkyl substituent $\text{CAAC}^{\text{Me}}\text{H}$. The $^1\text{H}\{^{11}\text{B}\}$ NMR spectrum shows a BH doublet at 1.90 ppm ($^3J = 6.6$ Hz), coupling to the BCH resonance of the $\text{CAAC}^{\text{Me}}\text{H}$ ligand at 4.38 ppm, as well as two sets of unsymmetrical CAAC^{Me} ligand resonances. An X-ray crystallographic analysis revealed a monomeric structure with a trigonal-planar boron atom ($\Sigma\angle\text{B1}$ 359(1) $^\circ$), in which the potassium cation bound to the BH hydride ($\text{K1}\cdots\text{H2}$ 2.53(3) Å) is encapsulated by the ligand sphere through $\eta^6-\pi$ interactions with the Dip (=2,6-diisopropylphenyl) substituents of the CAAC^{Me} and $\text{CAAC}^{\text{Me}}\text{H}$ ligands (Fig. 3). The $\text{B1}-\text{C1A}$ bond length of 1.439(11) Å is significantly shorter than in the 2- CAAC^{Me} precursor ($\text{B}-\text{C}_{\text{avg.}}$, 1.69 Å, Fig. 2) and typical of a $\text{B}=\text{C}$ double bond. This is indicative of strong π backdonation from the lone pair of the boryl anion to the π -accepting CAAC^{Me} ligand, as found in all CAAC-stabilised boryl anions.^{6,14-17} According to DFT calculations carried out at the $\omega\text{B97XD}/6-31+\text{G}^*$ level of theory, the HOMO of **5** possesses π -bonding character between B1 and C1A , with a nodal plane located at the $\text{C1A}-\text{N1}'$ bond region (Fig. 4). As in **3-DMAP**, a 1,2-hydride shift has occurred and C1B is now sp^3 -hybridised ($\text{B1}-\text{C1B}$ 1.633(9), $\text{N1}-\text{C1B}$ 1.520(8) Å). The presence of the hydrogen atom at boron was further confirmed by a solid-state infrared absorption at 2329 cm $^{-1}$, corresponding to the $\text{B}-\text{H}$ stretching mode. The computed $\text{B}-\text{H}$ stretching mode of 2352 cm $^{-1}$ at $\omega\text{B97XD}/6-31+\text{G}^*$ agrees well with the experimental value.

The reduction of 2- CAAC^{Me} in THF or the dissolution of **5** in THF both yielded the analogue **5-thf** (Scheme 2b, c and Fig. 3), in which the hydride-bound potassium cation is $\eta^6-\pi$ -stabilised now only by the Dip substituent of the neutral CAAC^{Me} ligand, its coordination sphere being completed by three THF molecules and an agostic interaction with one of the vicinal methyl groups (C25) of the $\text{CAAC}^{\text{Me}}\text{H}$ ligand. The bond lengths and

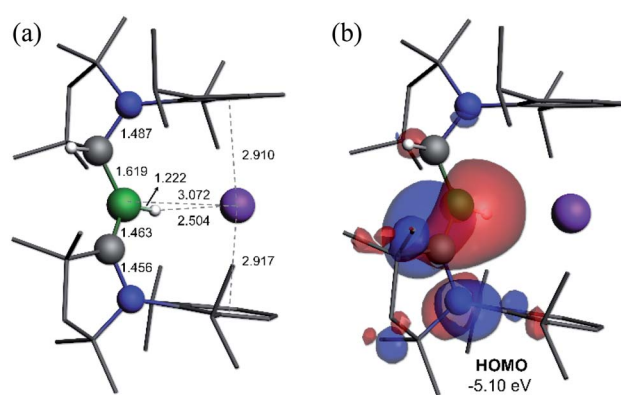


Fig. 4 (a) Calculated structure of **5** at the $\omega\text{B97XD}/6-31+\text{G}^*$ level of theory. (b) Plot of the HOMO of **5** ($\omega\text{B97XD}/6-311++\text{G}^{**}$).

angles of the boryl anion core change little compared to those of solvent-free **5**, the major difference being the conformation of the pyrrolidine rings of $\text{CAAC}^{\text{Me}}\text{H}$ and CAAC^{Me} , which flip so that the Dip substituents now point in opposite directions.

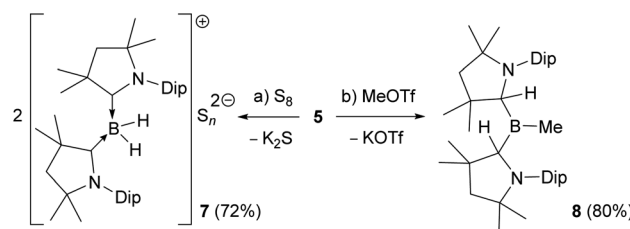
Cyclic voltammograms of 2- CAAC^{Me} and **5-thf** in THF (0.1 M $[\text{nBu}_4\text{N}]^{+}\text{[PF}_6^{-}]$) were essentially identical, showing a reversible redox event at $E_{1/2} = -2.31$ V and an irreversible oxidation around -0.90 V (relative to Fc/Fc^+), suggesting that chemical oxidation of **5** to **6** should be possible. Indeed, the reaction of **5-thf** with 2- CAAC^{Me} led to quantitative comproportionation to the boryl radical **6** (Scheme 2d). Attempts to generate **6** by the direct one-electron reduction of 2- CAAC^{Me} failed, resulting instead in incomplete consumption of 2- CAAC^{Me} and generating a mixture of **5** and **6**. Radical **6** is deep purple in solution ($\lambda_{\text{max}} = 523$ nm in the UV-vis spectrum) and ^{11}B NMR-silent. In the solid state, however, isolated crystals of **6** are deep orange. X-ray diffraction analysis showed a structure very similar to **5** bar the potassium cation, with a trigonal planar B1 centre ($\Sigma\angle\text{B1}$ 359.5(6) $^\circ$) and the Dip groups of the $\text{CAAC}^{\text{Me}}\text{H}$ and CAAC^{Me} ligands both pointing in the same direction (Fig. 3).



Unlike in **5** and **5-thf**, the B1–C1 and C1–N1 bonds at the neutral CAAC^{Me} ligand (1.5174(18) and 1.4601(18) Å, respectively) are within the range typical of partial double bonds, as is typical for CAAC-stabilised boryl radicals due to the delocalisation of the unpaired electron over the N1–C1–B1 π framework.^{5–9,21,22,31–33}

The IR spectrum of **6** shows a B–H stretching band at 2533 cm^{−1} (calc.: 2558 cm^{−1} at ωB97XD/6-31+G*), *ca.* 200 wavenumbers higher than that in **5**, and 100 higher than in Bertrand's hydroborylene **III** (Fig. 1a, ν (B–H) = 2455 cm^{−1}), suggesting a significant strengthening of the B–H bond in radical **6**. The EPR spectrum of **6** displays a broad triplet from the hyperfine coupling to the ¹⁴N nucleus ($a_{14\text{N}} = 18.5$ MHz, Fig. 5a). The simulated spectrum further provides hyperfine coupling parameters to the quadrupolar ¹¹B nucleus ($a_{11\text{B}} = 9.7$ MHz), which is responsible for the line-broadening, and the BH and CAAC^{Me}H ¹H nuclei ($a_{\text{H}} = 13.6$ and 4.8 MHz, respectively). The presence of two distinct couplings to these ¹H nuclei suggests that the compound displays no fluxional B-to-CAAC hydrogen migration in solution.

Calculations show that the SOMO consists mainly of the B1–C1 π bond with some π-antibonding character on the C1–N1 bond (Fig. 5c). The calculated Mulliken atomic spin densities are 53% on C1, 21% on N1 and only 15% on B1, showing that the unpaired electron is mainly delocalised on the CAAC ligand (Fig. 5d), as already suggested by the much stronger EPR hyperfine coupling to N1 than B1 (*vide supra*). To our knowledge, **6** is the first example of a neutral, structurally characterised hydroboryl radical. Moreover, to our surprise, isolated



Scheme 3 (a) Reducing and (b) nucleophilic reactivity of boryl anion **5**.

crystals of **6** proved air-stable at room temperature over a period of one week, making this compound a rare example of an air-stable boron-centred radical. This is presumably owed to a combination of the high degree of spin delocalisation, the low spin density at boron and the very effective encapsulation of the B–H unit by the CAAC^{Me} and CAAC^{Me}H ligands as seen in the electrostatic potential map in Fig. 5b. The only other air-stable boron-based radical reported is a permethylated icosahedral borane [*clos*-B₁₂(CH₃)₁₂][−] radical anion, in which the unpaired electron is trapped and delocalised within the B₁₂ cage.³⁴

Reactions of the boryl anion **5** with a wide range of electrophiles including haloboranes, organohalides, heavier group 14 chlorides, as well as Zn(II), Cu(I) and Au(I) halides all resulted in quantitative oxidation of **5** to radical **6**, and reduction of the corresponding electrophile. This contrasts with the boron nucleophile behaviour observed for CAAC-stabilised cyanoboryl anions.^{16,17} With elemental sulfur, double oxidation back to the 2-CAAC^{Me} cation was observed by NMR spectroscopic analysis ($\delta_{11\text{B}} = -22.4$ ppm, $t, J_{11\text{B}-1\text{H}} = 84.7$ Hz), the counteranion presumably being a S_n^{2-} polysulfide (**7**, Scheme 3a). The only nucleophilic reactivity observed was with methyl triflate, which yielded clean salt metathesis to the methylated trialkylborane **8** through migration of the second hydride to the remaining CAAC^{Me} ligand ($\delta_{11\text{B}} = 93.9$ ppm, Scheme 3b).

Conclusions

We have shown herein that the ability of CAACs to stabilise electron-rich boron centres and reversibly activate B–H bonds can be harnessed together to reduce a $[\text{L}_2\text{BH}_2]^+$ cation to a $[\text{LRBH}]^-$ anion without the usual need for halide abstraction, thanks to B-to-CAAC hydrogen shuttling. This boryl anion reacts principally as a one-electron reducing agent to yield the neutral hydroboryl radical $[\text{LRBH}]^{\cdot}$, the surprising stability of which is ensured by the unique stereoelectronic properties of the two encapsulating CAAC^{Me} ligands.

Conflicts of interest

The authors declare no conflict of interest.

Acknowledgements

The authors thank the Deutsche Forschungsgemeinschaft for financial support. S. H. is grateful for a doctoral fellowship from

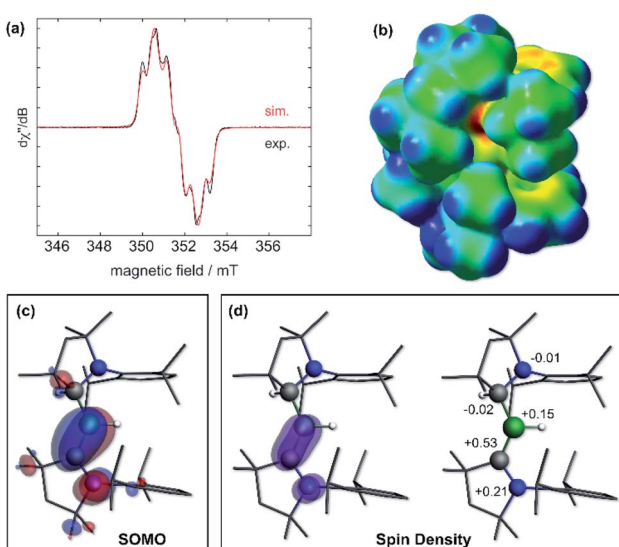


Fig. 5 (a) Experimental (black solid line) and simulated (red line) continuous-wave X-band EPR spectra of **6** in hexane solution at rt. *Simulation parameters:* $g_{\text{iso}} = 2.0027$, $a^{11\text{B}} = 9.7$ MHz, $a^{14\text{N}} = 18.5$ MHz, $a^{1\text{H}_{(\text{H}1)}} = 13.6$ MHz and $a^{1\text{H}_{(\text{H}21)}} = 4.8$ MHz; (b) electrostatic potential (ESP) map of **6** at the ωB97XD/6-31+G* level of theory. ESP charges following the notation of Fig. 3: N2: −0.46, C21: −0.01, B1: +0.19, H1: −0.17, C1: −0.27, N1: −0.14. (c) Plot of the SOMO of **6** (surface isovalue: ± 0.03 [$e \text{a}_0^{-3}$]^{1/2}). (d) Left: plot of the calculated spin density of **6** (surface isovalue: 0.005 [$e \text{a}_0^{-3}$]). Right: Mulliken atomic spin densities.



the Studienstiftung des Deutschen Volkes. F. F. thanks the Coordenação de Aperfeiçoamento de Pessoal de Nível Superior (CAPES) and the Alexander von Humboldt (AvH) Foundation for a Capes-Humboldt postdoctoral fellowship.

Notes and references

‡ The boron-bound hydrides of each structure were detected as residual electron density in the difference Fourier map and freely refined.

§ The X-ray crystallographically-determined structures of **1**, **2-Pyr** and **2-DMAP** can be found in the ESI, Fig. S55–S57.†

- 1 S. Kundu, S. Sinhababu, V. Chandrasekhar and H. W. Roesky, *Chem. Sci.*, 2019, **10**, 4727.
- 2 U. S. D. Paul, M. J. Krahfuß and U. Radius, *Chem. Unserer Zeit*, 2018, **53**, 212.
- 3 M. Melaimi, R. J. M. Soleilhavoup and G. Bertrand, *Angew. Chem., Int. Ed.*, 2017, **56**, 10046.
- 4 M. Soleilhavoup and G. Bertrand, *Acc. Chem. Res.*, 2015, **48**, 256.
- 5 Y. Su and R. Kinjo, *Coord. Chem. Rev.*, 2017, **352**, 346.
- 6 M. Arrowsmith, J. I. Schweizer, M. Heinz, M. Härterich, I. Krummenacher, M. C. Holthausen and H. Braunschweig, *Chem. Sci.*, 2019, **10**, 5095.
- 7 H. Braunschweig, I. Krummenacher, M.-A. Légaré, A. Matler, K. Radacki and Q. Ye, *J. Am. Chem. Soc.*, 2017, **139**, 1802.
- 8 F. Dahcheh, D. Martin, D. W. Stephan and G. Bertrand, *Angew. Chem., Int. Ed.*, 2014, **53**, 13159.
- 9 P. Bissinger, H. Braunschweig, A. Damme, I. Krummenacher, A. K. Phukan, K. Radacki and S. Sugawara, *Angew. Chem., Int. Ed.*, 2014, **53**, 7360.
- 10 J.-S. Huang, W.-H. Lee, C.-T. Shen, Y.-F. Lin, Y.-H. Liu, S.-M. Peng and C.-W. Chiu, *Inorg. Chem.*, 2016, **55**, 12427.
- 11 S. Kumar Sarkar, M. M. Siddiqui, S. Kundu, M. Ghosh, J. Kretsch, P. Stollberg, R. Herbst-Irmer, D. Stalke, C. Stückl, B. Schwederski, W. Kaim, S. Ghorai, E. D. Jemmis and H. W. Roesky, *Dalton Trans.*, 2019, **48**, 8551.
- 12 D. A. Ruiz, M. Melaimi and G. Bertrand, *Chem. Commun.*, 2014, **50**, 7837.
- 13 R. Kinjo, B. Donnadieu, M. A. Celik, G. Frenking and G. Bertrand, *Science*, 2011, **333**, 610.
- 14 M. Arrowsmith, J. D. Mattock, S. Hagspiel, I. Krummenacher, A. Vargas and H. Braunschweig, *Angew. Chem., Int. Ed.*, 2018, **57**, 15272.
- 15 M. Arrowsmith, J. D. Mattock, J. Böhnke, I. Krummenacher, A. Vargas and H. Braunschweig, *Chem. Commun.*, 2018, **54**, 4669.
- 16 M. Arrowsmith, D. Auerhammer, R. Bertermann, H. Braunschweig, M. A. Celik, J. Erdmannsdörfer, I. Krummenacher and T. Kupfer, *Angew. Chem., Int. Ed.*, 2017, **56**, 11263.
- 17 D. A. Ruiz, G. Ung, M. Melaimi and G. Bertrand, *Angew. Chem., Int. Ed.*, 2013, **52**, 7590.
- 18 J. Böhnke, M. Arrowsmith and H. Braunschweig, *J. Am. Chem. Soc.*, 2018, **140**, 10368.
- 19 M. Arrowsmith, D. Auerhammer, R. Bertermann, H. Braunschweig, G. Bringmann, M. A. Celik, R. D. Dewhurst, M. Finze, M. Grüne, M. Hailmann, T. Hertle and I. Krummenacher, *Angew. Chem., Int. Ed.*, 2016, **55**, 14462.
- 20 M. Soleilhavoup and G. Bertrand, *Angew. Chem., Int. Ed.*, 2017, **56**, 10282.
- 21 M.-A. Légaré, M. Rang, G. Bélanger-Chabot, J. I. Schweizer, I. Krummenacher, R. Bertermann, M. Arrowsmith, M. C. Holthausen and H. Braunschweig, *Science*, 2019, **363**, 1329.
- 22 M.-A. Légaré, G. Bélanger-Chabot, R. D. Dewhurst, E. Welz, I. Krummenacher, B. Engels and H. Braunschweig, *Science*, 2018, **359**, 896.
- 23 M.-A. Légaré, C. Pranckevicius and H. Braunschweig, *Chem. Rev.*, 2019, **119**, 8231.
- 24 C. Hering-Junghans, *Angew. Chem., Int. Ed.*, 2010, **57**, 6738.
- 25 A. J. Ruddy, D. M. C. Ould, P. D. Newman and R. L. Melen, *Dalton Trans.*, 2018, **47**, 10377.
- 26 D. Auerhammer, M. Arrowsmith, H. Braunschweig, R. D. Dewhurst, J. O. C. Jiménez-Halla and T. Kupfer, *Chem. Sci.*, 2017, **8**, 7066.
- 27 M. Arrowsmith, J. Böhnke, H. Braunschweig and M. A. Celik, *Angew. Chem., Int. Ed.*, 2017, **56**, 14287.
- 28 S. Würtemberger-Pietsch, H. Schneider, T. B. Marder and U. Radius, *Chem. -Eur. J.*, 2016, **22**, 13032.
- 29 M. R. Momeni, E. Rivard and A. Brown, *Organometallics*, 2013, **32**, 6201.
- 30 G. D. Frey, J. D. Masuda, B. Donnadieu and G. Bertrand, *Angew. Chem., Int. Ed.*, 2010, **49**, 9444.
- 31 A. Deißenberger, E. Welz, R. Drescher, I. Krummenacher, R. D. Dewhurst, B. Engels and H. Braunschweig, *Angew. Chem., Int. Ed.*, 2019, **58**, 1842.
- 32 J. Böhnke, T. Dellermann, M. A. Celik, I. Krummenacher, R. D. Dewhurst, S. Demeshko, W. C. Ewing, K. Hammond, M. Heß, E. Bill, E. Welz, M. Röhr, R. Mitić, B. Engels, F. Meyer and H. Braunschweig, *Nat. Commun.*, 2018, **9**, 1197.
- 33 M. Arrowsmith, J. Böhnke, H. Braunschweig, M. A. Celik, C. Claes, W. C. Ewing, I. Krummenacher, K. Lubitz and C. Schneider, *Angew. Chem., Int. Ed.*, 2016, **55**, 11271.
- 34 T. Peymann, C. B. Knobler and M. F. Hawthorne, *Chem. Commun.*, 1999, 2039.

